KU LEUVEN

FACULTY OF SCIENCE

Investigating asteroseismic post-mass transfer candidates using population synthesis

İremsu TAŞKIN

Supervisor: Dr. Alex Kemp
KU Leuven Institute of Astronomy

Mentor: Annachiara Picco
KU Leuven Institute of Astronomy

Master thesis submitted in fulfillment
of the requirements for the degree in
Master of Science in Astronomy and Astrophysics

Academic year 2023-2024

Preface

This study would not be possible if not for the many people of IvS who have scientifically or emotionally contributed to the many facets of this paper.
I would like to start by thanking Dr. Alex Kemp and Annachiara Picco. Without our long meetings of trying to troubleshoot the same problem multiple weeks in a row and discussing the many intricacies of how I must be doomed by the narrative for the most trivial reasons, I believe I would not be able to conclude this study in any way. Thank you for spending so much of you time on me again and again, and thank you for guiding me in every step.
I would also like to thank the second year masters students of 2024 for struggling with me at any minor inconvenience. The many nights we have spent together working on papers not only got me through the many hurdles of a masters degree, but also made precious memories to look back on in the future. May the future hold many more dates at IvS for us.
Finally I would like to thank my family for supporting me no matter how steadfast I have been on this uncertain road. I was in middle school when I decided to study astronomy and make it my life for however long I could. However, my many attempts fell short. You have probably heard enough of me and my complaints about not being where I wanted to be for years. However, now that I have taken my first step into a life intertwined with astronomy, I hope you are enjoying your moment of peace. I would like to especially thank my parents who were supportive of me in every way my whole life.
Finally, she does not know how to read and I am sure she would not care if she could, but I would like to thank my cat Ponyo. You are truly an interesting specimen that brightens my life.

Scientific Summary

Context. Binary systems dominate the universe, as most stars are born in binaries. The evolution of stars within these systems are fundamentally different from that of single stars. Past observations by Rui and Fuller (2021); Li et al. (2022) as well as models by Deheuvels et al. (2022) have shown cases of stars on the Giant Branch that have degenerate cores but disproportionately massive envelopes. These studies have attributed the behavior of the Giant Branch stars to possible mass transfer in its lifetime with a companion star.

Aim. This study utilizes the theoretical background from Deheuvels et al. (2022) and Rui and Fuller (2021) to use binary population synthesis and analyze the behavior of stars during and after mass transfer. The common channels leading to the formation of these stars, the trends in the binary system parameters and the behavior of the companion star are studied. The significance of each binary interaction type on seeking post-mass transfer stars in the nature is estimated to get a better understanding of the observability of this phenomenon.

Methodology. Binary population synthesis code `binary_c` is used to generate large populations of binary systems. Multiple simulations are run in order to see the effects of various binary physics such as α_{CE}, wind Roche lobe overflow and metallicity. Each population is analyzed and classified using the single star models of each star to obtain an expected single star evolution and compare it to the binary evolution to identify discrepancies. Through this classification, various channels are identified. These results are weighed with respect to the birth probabilities of the stars to have a better understanding of how these events reflect to the nature and their significance for future observations.

Results. Multiple channels are identified across the population, each densely populated in certain parts of the initial parameter space. Cases of mergers with smaller Main Sequence companions dominate in terms of systems per unit star forming material. Many cases of Roche lobe overflow and wind mass transfer are observed, all originating from systems where the stars accrete material from a companion TPAGB star shedding its envelope. The classification scheme is found to be minimally sensitive to the degeneracy conditions. However, the mass transfer conditions provide large variations across each classification. The physics cases probing α_{CE} proved to affect the mergers drastically while the wind Roche lobe overflow case created a population where wind mass transfer and Roche lobe overflow events were dominating. Probing the metallicity provided an idea of how binary interactions may be affected, but it is too complex to infer. High resolution analysis was attempted, but showed traces of possible oversampling.

Summary for General Audience

Stars are usually not born alone. They are commonly part of a binary system for most of their lives, evolving together and interacting. We can not track these interactions most of the time, but we can infer their existence through the changes they have caused to the stars themselves.

In this study, I attempt to identify stars that have experienced mass transfer in their lifetimes by analyzing their stellar parameters as they evolve. As low-mass stars evolve as singles, they develop degenerate cores. However, in a binary system, a low-mass star can accrete material onto itself from its companion, leading to an increased mass but an unchanged, degenerate core. Their degenerate cores make them differ from a more massive stars with similar mass after the mass transfer event, as these massive stars do not develop degenerate cores.

Using simulations of large populations, I identify which stars show the characteristics of a post-mass transfer star. Afterwards, I analyze the interactions in the binary system to see which types of interactions lead to the formation of these post-mass transfer stars. Normalizing them using the birth probabilities of each system, I am able to analyze how probable it is to observe the stars formed out of these events in nature.

Contribution Statement

I would like to thank Dr. Alex Kemp for his contributions in navigating `binary_c` and providing me with the base codes to build up onto. I would also like to thank Annachiara Picco for her work on the `MESA` models.
I would like to thank Dr. Robert Izzard for his work on `binary_c`, which is the backbone of this study, as well as all the contributors through which I could conduct my research. I would also like to thank everyone who tirelessly worked on developing `MESA`.

Glossary

$\Delta\nu$ asymptotic large separation.

$\Delta\Pi_1$ asymptotic period spacing.

ρ density.

T_{eff} effective temperature of star.

$\xi(M)$ Initial Mass Function.

L luminosity of star.

P period of the binary system.

R_d wind accretion zone radius.

R_L Roche radius.

q mass ratio.

Acronyms

MESA Modules for Experiments in Stellar Astrophysics.

BPS Binary Population Synthesis.

BSE Binary Star Evolution.

CE Common Envelope.

CHeB Core He-burning.

COWD Carbon Oxygen White Dwarf.

GB Giant Branch.

HG Hertzsprung Gap.

HR Hertzsprung-Russell.

IMF Initial Mass Function.

MR Massless Remnant.

MS Main Sequence.

MT mass transfer.

RLOF Roche lobe overflow.

SSE Single Star Evolution.

TAMS Terminal Age Main Sequence.

TPAGB Thermally Pulsing Asymptotic Giant Branch.

usfm unit star forming material.

WD White Dwarf.

WRLOF wind Roche lobe overflow.

ZAMS Zero Age Main Sequence.

List of Figures

List of Tables

Contents

Chapter 1

Introduction

Most stars are born in binaries (Sana et al., 2012), with most massive stars displaying high multiplicity fractions (Izzard et al., 2006; Sana, 2017). The difficulty of detecting low-mass companions ($M_* \approx 0.1 - 0.5 M_\odot$) in a binary system makes it challenging to study the multiplicity of intermediate-mass stars ($M_* \approx 0.5 - 5 M_\odot$) (Duchêne and Kraus, 2013). However, studies of spectroscopic binaries (Abt, 1983) as well as surveys searching for visual binaries (Kouwenhoven et al., 2005; De Rosa et al., 2011) lead to an estimation of multiplicity frequency $\geq 50\%$ for intermediate stars (Duchêne and Kraus, 2013).

According to Podsiadlowski et al. (1992), only $30 - 50\%$ of the systems experience binary interactions. Nonetheless, interactions between a star and its companion dominate the evolution of the star (Sana et al., 2012). Thus, the evolution of stars within binary systems differ from that of their single counterparts. Recent studies focus on the identification of these differences and their observability.

Single stars evolve along the Hertzsprung-Russell (HR) diagram, climbing the Giant Branch (GB) until they experience a Helium flash. As these stars evolve, their core properties change. Lower mass stars have a degenerate core up until the end of GB (Pols et al., 1998; Hurley et al., 2000) while intermediate-mass stars have non-degenerate cores during the GB (Deheuvels et al., 2022). Studies conducted using Modules for Experiments in Stellar Astrophysics (MESA) models (Deheuvels et al., 2022) and catalogs of observed GB stars (Rui and Fuller, 2021; Li et al., 2022) have shown systems hosting GB stars with core properties deviating from what is expected for single stars evolving along the HR diagram. This study builds upon the findings of Deheuvels et al. (2022) and Rui and Fuller (2021).

1.1 Stellar Evolution

This section is heavily based on Aerts (2021) and Pols (2011b).

Stars are born in the dense regions of the interstellar medium, through the collapse of molecular clouds. Under the dominating gravitational force, molecular clouds fragment and these fragments contract until a protostar is formed.

To understand stellar evolution from the protostar stage up until the death of the star, we need to take a close look at the HR diagram. The HR diagram (Figure 1.1) correlates the observable properties of a star, namely its luminosity L and effective surface temperature T_{eff} (Hurley et al., 2000).

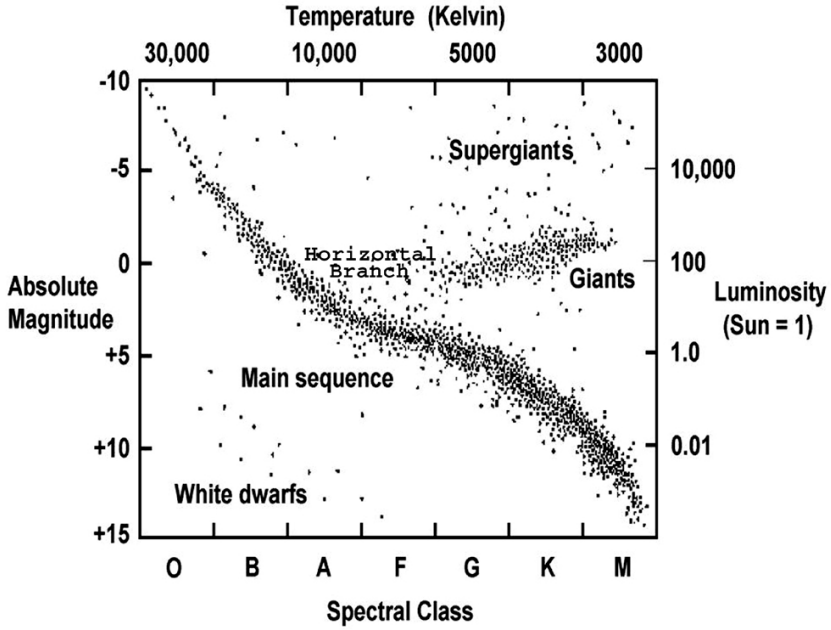

Figure 1.1: Diagram by Chandra (2015)

The evolution of the star and the length of its lifetime heavily depend on said star's mass. The difference in the evolutionary tracks of stars with different masses is visualized in Figure 1.2. This highlights the fact that the mass of the star is a determining factor on what stellar types it will become as it evolves, as well as the end product of its life. The distribution of stars with respect to their masses was quantified by Salpeter (1955) using observation data, eventually defining the Initial Mass Function (IMF) $\xi(M)$ as follows.

$$\xi(M) \sim \left(\frac{M}{M_{\odot}}\right)^{(-1.35\pm0.3)} \tag{1.1}$$

The rest of this section will focus on the stages in the evolution of a single star. As the discrepancies identified by Deheuvels and Michel (2011) and Rui and Fuller (2021) are in populations of intermediate-mass and low-mass stars, we will track the evolution of a low-mass star in detail. The differences for intermediate-mass and high-mass stars (Aerts, 2021) will be briefly discussed in relation to the low-mass star evolution.

1.1.1 Early Stellar Evolution

Upon the formation of a protostar, it continues to contract with constant T_{eff} and decreasing radius. Consequently, the central density and central temperature of the star increase until the gas is ionized (Aerts, 2021) and a pre-MS star is formed.

The pre-MS star will first start deuterium burning, followed by hydrogen burning. The burning of hydrogen brings the star into equilibrium and the star ceases its contraction (Pols, 2011b). The time at which equilibrium is achieved is referred to as Zero Age Main Sequence (ZAMS). Stars that have reached ZAMS are fully homogeneous and in both hydrostatic and thermal equilibrium. Thus, they follow a given mass-luminosity relation (Equation 1.3).

$$L \propto \mu^4 M^{3.3} \tag{1.2}$$

Stars burn hydrogen in their cores to form helium (Hurley et al., 2000), which is their primary source of energy production throughout the MS. Formation of helium leads to an increase in the core molecular weight μ_c. Consequently, the luminosity of the star shows a drastic increase as per the relation in Equation 1.3. This increase in luminosity can be tracked in Figure 1.2, in between ZAMS and the end of core hydrogen burning.

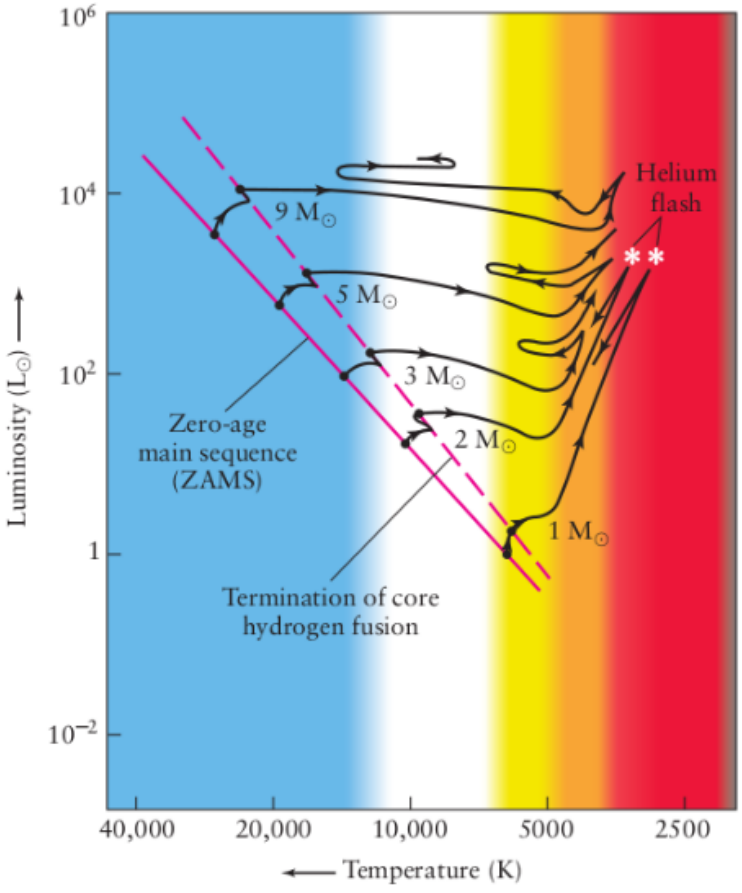

Figure 1.2: Evolution of stars from ZAMS to Helium flash on HR diagram (Comins and Kaufmann, 2008).

As the energy produced by hydrogen burning is heavily dependent on the temperature, the layers of MS stars show varying properties. Stars with $(M_* \leq 0.35 M_\odot)$ are fully convective while

stars with $(0.35M_{\odot} < M_{*} \leq 1.2M_{\odot})$ have radiative cores enveloped by a convective zone. Conversely, more massive stars of $(M_{*} > 1.2M_{\odot})$ have convective cores and radiative envelopes (Pols, 2011b). The convective cores of these more massive stars are directly correlated to the stellar interior's steep temperature gradient (Hurley et al., 2000)

Most of a star's lifetime is spent on the MS, with the exact MS time τ_H being heavily dependent on its mass. Using the mass luminosity relation referred to in Equation 1.3, we can define τ_H as a function of mass.

$$\tau_H\left(M\right) \propto \frac{M}{L} \propto M^{-2.3} \tag{1.3}$$

The mass dependence of τ_H shows that the MS lifetime of a star drastically increases as the mass decreases (Aerts, 2021). Stars remain in the MS until they exhaust all of their hydrogen resources in their cores. This is referred to as the TAMS, where core hydrogen burning is terminated (Figure 1.2).

1.1.2 Post-MS evolution

At the end of the MS, the star is left with a core that has exhausted all hydrogen with a surrounding envelope rich in hydrogen. Post-MS evolution varies greatly between stars of different masses, as discussed previously.

Low mass stars of $M_{*} \leq 2M_{\odot}$ develop a dense and cool helium core. The electrons in the core are partially degenerate, allowing the core to stay in equilibrium. As the star switches from core to shell hydrogen burning, the core contracts and the envelope expands. By the time the star reaches GB, the core is degenerate and the envelope is mostly convective (Pols, 2011b). Looking at the HR diagram (Figure 1.1) and the evolution tracks (Figure 1.2), this process shows a decrease in temperature while the luminosity remains almost constant.

These stars have a long Red GB phase during which they experience a strong increase in radius. This causes a strong increase in the luminosity and the star starts climbing the HR diagram along the GB. Upon reaching the tip of the GB, the core starts to contract and its temperature increases. The star experiences an abrupt helium flash which removes degeneracy and eventually leads to stable helium burning in the core Hurley et al. (2002).

Unlike low-mass stars, intermediate stars do not have a degenerate helium core. Instead, they form a degenerate carbon-oxygen core following the end of core helium burning. High mass stars also have a non-degenerate core and ignite carbon. Stars of very high masses are able to reach central temperatures high enough to ignite helium before Hertzsprung Gap (HG) and thus skip the GB.

Eventually, low-mass and intermediate-mass stars shed their envelopes and end up as White Dwarf (WD). High mass stars, on the other hand, keep burning heavier elements until they collapse. The collapsing core sends a shockwave that ejects its envelope in an event called supernova. The inner core can end up as a neutron star or collapse into a black hole (Hurley et al., 2002).

1.2 Binary Evolution

This section is heavily based on Pols (2011a).

While single stars follow their evolutionary tracks as displayed in Figure 1.2, binary stars experience many additional effects that affect their evolution both for the stars themselves and as a system. Any interactions between the stars within the system can affect the fundamental parameters of the system as a whole, such as the separation and eccentricity. In a similar vein, it can change the evolutionary tracks the stars follow. We can focus on the two important aspects binary evolution and the possible interactions.

1.2.1 Stable Mass Transfer

The Roche model states that each body in a binary system has a zone of influence within which a test particle will remain gravitationally bound to the body. Kopal (1978, 1989) further describes this as material within the zone of influence remains bound to the body while any material outside this zone can be accreted onto the companion. This is called the Roche potential.

The equipotential surfaces in the Roche potential produce the Roche geometry illustrated in Figure 1.3. The points of equilibrium, called Lagrange points, are denoted with the letter L. In particular, the equipotential line passing through L_1 defines the two Roche lobes around each star (Pols et al., 1998). The radius of these lobes are dependent on the mass ratio between the stars $q = M_2/M_1$ and their separation a, defined as follows.

$$\frac{R_{L,1}}{a} = \frac{0.49q^{2/3}}{0.6q^{2/3} + \ln 1 + q^{1/3}} \tag{1.4}$$

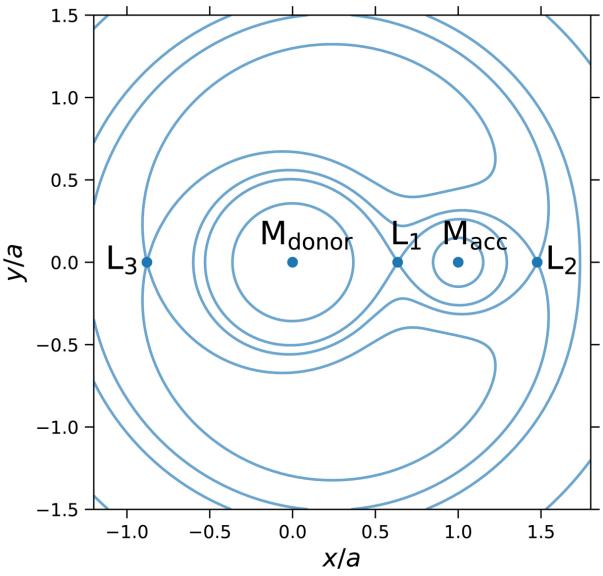

Figure 1.3: Equipotential lines of Roche potential for a binary system by Misra et al. (2020).

This geometry has three possible configurations:

- **Detached binary** where stars exist in an equipotential surface within their respective Roche lobes, leading to minimal interaction. These stars can be approximated to single stars.

- **Semi-detached** where only one of the stars fills its Roche lobe. If the star keeps growing, material will be accreted onto the companion through L_1.This process if Roche lobe overflow (RLOF).

- **Contact binary** where both stars fill their Roche lobes and keep expanding. They eventually fill an equipotential surface between L_2 and L_1.

As another mass transfer (MT) mechanism, Abate et al. (2013) highlights that in the presence of slow and dense winds, efficient wind transfer can be conducted through a process called WRLOF. In this method, wind from the primary is focused on the secondary. This results in a dramatic increase in the expected accretion rate. However, the runoff material from this mechanism leads to the loss of angular momentum (Abate et al., 2013).

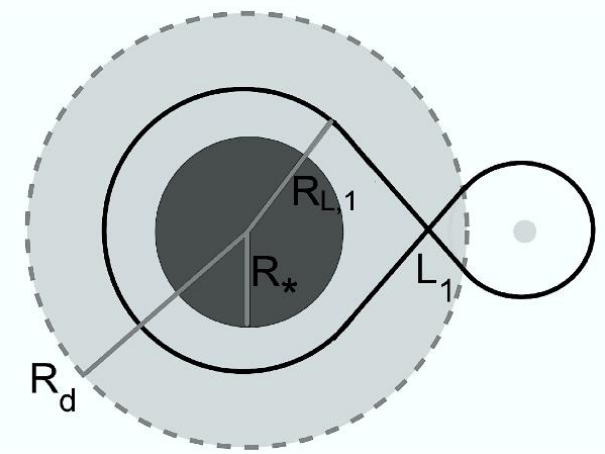

Figure 1.4: Wind Roche lobe overflow mechanism (Abate et al., 2013).

1.2.2 Unstable Mass Transfer

Stability of MT in a RLOF event is dependent on the response of the donor radius, the response of the companion star and the response of the binary orbit (Pols, 2011a). In cases of unstable MT, the MT rate increases uncontrollably as the donor outgrows its Roche lobe. This can lead to Common Envelope (CE) events. CE events are typically observed in binaries with high q where the donor has a convective envelope or in binaries with very low mass ratios with the donor having a radiative envelope.

In the CE setting, the accretor within the envelope of the donor creates friction between itself and the envelope as it moves. This friction leads to the loss of angular momentum and the orbit starts to shrink. In this shrinking process, the envelope is heated and gains energy. If enough energy is transferred to the envelope, it can be shed. However, if not enough energy is produced, the orbit continues to shrink, eventually leading to the accretor merging with the core of

the donor.

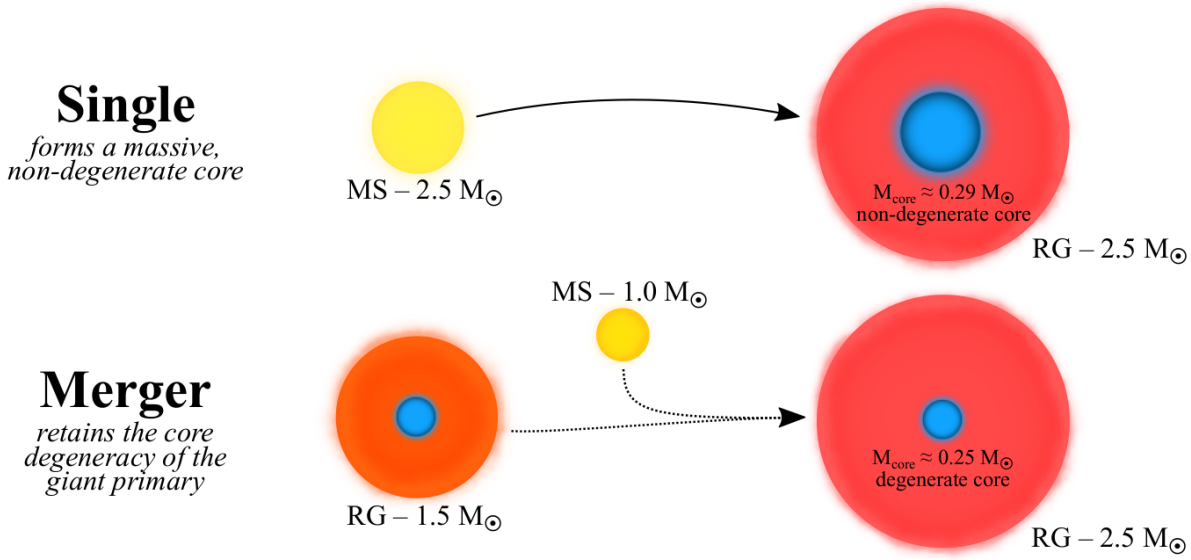

Figure 1.5: Illustration of single star evolution compared to binary merger by Rui and Fuller (2021).

The products of these CE events vary depending on the types of the stars involved as well as the stellar parameters such as their masses. In the context we are interested in, a GB star can merhe with a MS star, only adding material onto its envelope and keeping its core mostly unaffected. This can produce a GB with a degenerate core and overmassive envelope, as illustrated in Figure 1.5.

1.3 Asteroseismology

This section is heavily based on Aerts et al. (2010).

Asteroseismology allows us to probe the insides of stars using the acoustic waves present in the stars reflecting from the surface of the star to the inner regions of the star and back. Aerts et al. (2010) describes this process as the lower part of the wave being in a hotter environment with a higher sound speed and thus refracting from this environment back to the surface, where it is reflected back into the star. These waves penetrate different depths of the star. This allows us to map the inside of the star in terms of the sound speed and obtain the temperature profile.

There are two types of pulsation modes which allow for the asteroseismic observations. These are p-modes that are the pressure modes and g-modes that are the gravity modes. The p-modes are significant for the outer zones of the part while the g-modes perturb the interior of the star.

Asymptotic relations in stars are important to understand the behavior of the stars. Using the p-mode frequencies provided by Tassoul (1980); Tassoul et al. (1990), we can derive $\Delta\nu$, the large separation. This is the inverse of the time it takes for a sound wave to travel from the

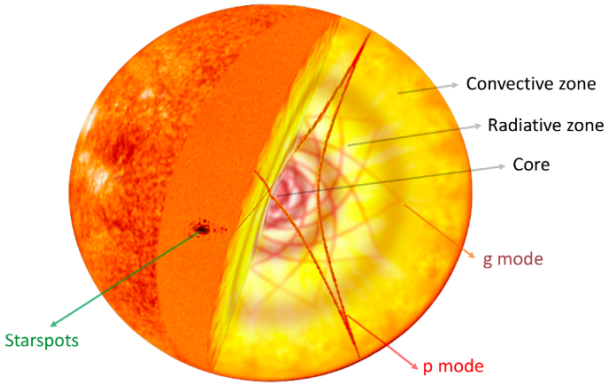

Figure 1.6: Diagram by García and Ballot (2019) showing the cross section of a $1M_{\odot}$ star. The star is divided in two with an inner radiative zone including the core and an outer convective zone. The mixed mode propagation of g-modes and p-modes are illustrated.

surface to the core and back.

$$\Delta\nu = \left(2\int_0^R \frac{dr}{c\,(r)}\right)^{-1} \tag{1.5}$$

where $c\,(r)$ is the sound speed. $\Delta\nu$ is sensitive to the radius of the star, as seen in Equation 1.5. From the periods of the g-modes, we can obtain the period spacings for the g-modes.

$$\Pi_1 = \pi^2\sqrt{2}\left(\int \frac{N_{BV}}{r}\,dr\right)^{-1} \tag{1.6}$$

where N_{BV} is the Brunt-Väisälä frequency. The integral is taken over the region where the g-mode propagates. The p and g-modes are illustrated in Figure 1.6.

In GB stars in particular, mixed modes are observed where p-modes and g-modes are coupled. These mixed modes are sensitive to both the envelope and core properties of the star, allowing observers to have an in depth understanding of the stellar interior Hekker et al. (2006); Deheuvels et al. (2022) through high-precision space photometry.

In Figure 1.7, Deheuvels et al. (2022) shows the relationship between the $\Delta\Pi_1$ and the ρ of a star. Given the fact that our interests lie in the population of stars that have degenerate cores and overmassive envelopes, we can probe this discrepancy asteroseismically, which allows us to have observations for these stars.

The core degeneracy of a star and when in its evolution it becomes degenerate are heavily dependent on the mass as discussed in Section 1.1.1. Thus, $\Delta\Pi_1$ also carries this mass dependency. Analyzing the relationship of the two asymptotic relations, Deheuvels et al. (2022) illustrate that they can identify populations of stars deviating from their expected track. These findings point to the observability of the stellar parameters that point to a past MT event in the star's lifetime.

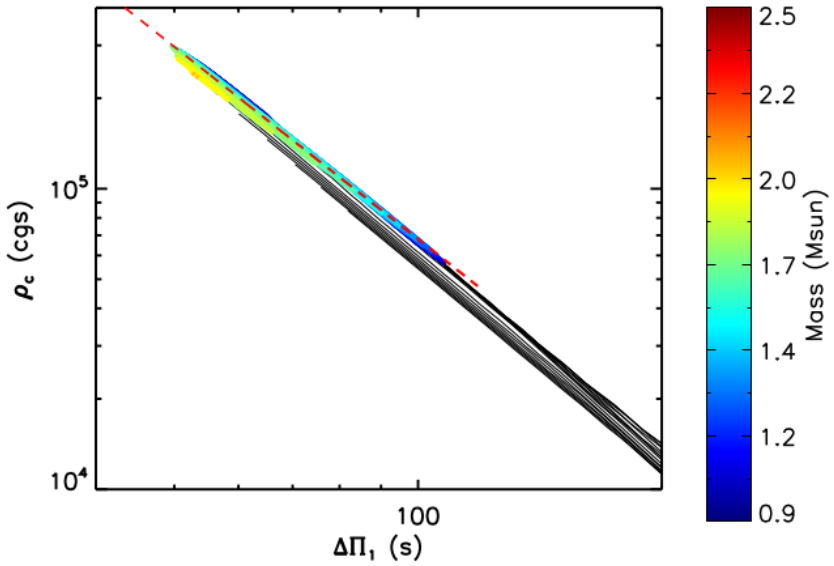

Figure 1.7: $\Delta\Pi_1$ - ρ_c plot by Deheuvels et al. (2022) showing the relationship between $\Delta\Pi_1$ and core density ρ_c. The colored lines correspond to evolution periods with high electron degeneracy in the core. In contrast, the black lines correspond to evolution periods with low core electron degeneracy. The red dashed line represents the linear regression of the $\Delta\Pi_1$ - ρ_c relation in stars that have degenerate cores.

Motivated by the reflection of the parameters of a post-MT star on asteroseismic behaviors that can be observed, I focus my study on the trends in these stars and the channels that lead them to becoming post-MT stars. For this purpose, I use binary population synthesis to obtain large samples of binaries and rigorously analyze various physics of binary evolution to see its effects on the systems.

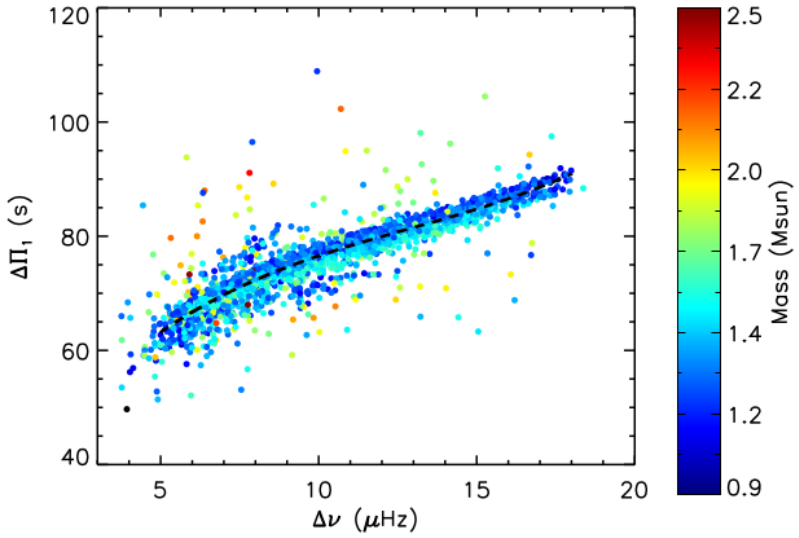

Figure 1.8: $\Delta\nu$ - $\Delta\Pi_1$ relation of GB stars by Deheuvels et al. (2022). Core He-burning (CHeB) stars with $\Delta\Pi_1$ above 130s are not included. The dashed black line represents the average distribution of GB stars obtained from observations.

Chapter 2

Methods

Stellar models and simulations play a crucial role in understanding the evolution of a star. The modelling of single stars is simplified by the fact that they can be approximated to 1-D balls of gas Izzard et al. (2006). These simulations are able to calculate the various parameters of a star as it evolves. However, single star evolution models do not provide the unique evolutionary pathways produced by binary systems (Eldridge et al., 2017). In a similar vein, these single star simulations are not able to account for the effects of binary interactions. In order to remediate this, various Binary Population Synthesis (BPS) focusing on binary interactions have been developed.

This study uses population synthesis to identify binary interactions within systems and channels that lead to the formation of stars with core-envelope discrepancies.

2.1 Population Synthesis

BPSs generate an initial binary population and efficiently evolve each system in the population using various methods. Due to the computational weight of modelling binary systems to calculate their evolution, most BPSs do not directly compute the evolution of each star. Parametric BPS approximate stellar evolution using look-up tables or fitting formulae which are based on preexisting single star models (Fragos et al., 2023). Binary interactions within the system are then modeled using various prescriptions.

In this study, I use `binary_c` [1] to generate large populations of binary systems. `binary_c` is a population nucleosynthesis code by Izzard et al. (2004, 2006, 2009, 2018) that synthesizes populations of binaries based on the Binary Star Evolution (BSE) code of Hurley et al. (2002). It creates a grid of binary systems using initial value ranges of M_1, q and P and sampling them according to the given resolution. The grid parameters used in the various populations generated for this study are displayed in Table 2.1.

BSE uses fitting formulae and subroutines to compute single stellar evolution properties based on Single Star Evolution (SSE) (Hurley et al., 2000). Using these evolution calculations and by modeling binary physics, it is able to compute parameters of systems through binary evolution (Agrawal et al., 2023). By providing access to various binary system prescriptions,

[1] https://binary_c.gitlab.io/

Parameter	Range	Sampling Function	Resolution
M_1	$0.8M_\odot$–$4M_\odot$	uniform	60
q	0.01-1	uniform	60
P	10^{-1} days–10^6 days	uniform	60

Table 2.1: Initial parameter space for binary population synthesis.

`binary_c` produces and evolves large populations of binaries in a relatively fast pace. It allows for the freedom of disregarding certain binary physics or using different prescriptions for different physics. The specific prescriptions in addition to BSE and the constants of certain binary parameters that were used in these populations are listed in Table 2.2.

Variable / Physics	Prescription
Eccentricity at birth	0
Simulation time	13700 MYr
RLOF model	Claeys et al. (2014)
CE binding energy λ	Dewi and Tauris (2000); Tauris and Dewi (2001)
Critical mass ratio q_{crit}	Hurley et al. (2002) [2]
Wind mass loss	Comerford and Izzard (2020)
GB winds	Hurley et al. (2000, 2002)
Thermally Pulsing Asymptotic Giant Branch (TPAGB) winds	Karakas et al. (2002) [3]

Table 2.2: Scientific parameters in the model used for population synthesis.

2.1.1 Simulation Physics

To analyze the effects of various binary physics on binary interactions and consequently the formation of stars with overmassive envelopes, I generate multiple populations with different physics. As my baseline, I use a population with no additional prescriptions to Table 2.2. In this fiducial case, I disregard WRLOF, use a solar metallicity of Z 0.02 and keep $\alpha_{CE} = 1$. In the additional physics cases, I toggle these parameters one by one to see their effects on the population. Each one of these parameters and their significance are further discussed in this section.

Metallicity of a star is a reflection of the elemental abundance of the star. Thus, it affects many evolutionary parameters and thus the binary interactions. While an analysis of the direct effects of metallicity is very complex, I generate an additional population of Z 0.02 to briefly analyze and visualize this.

CE Evolution

RLOF can lead to a binary system forming a CE in certain cases. Within BSE, there are two channels producing CE events; a collision between a star with a dense core and its companion, or RLOF from a giant star where the system satisfies $q_1 > q_{crit}$ (Hurley et al., 2002) where q_1 is the q of the primary star.

[2] Modified from Reimers (1975)
[3] Modified from Vassiliadis and Wood (1993)

The product of a CE event depends on the initial envelope binding energy $E_{bind,i}$ and the initial orbital energy $E_{orb,i}$ of the system (Tout et al., 1997; Hurley et al., 2002). In a CE event, the two stellar cores transfer their orbital energy to the envelope as they spiral in. This event occurs at an efficiency of α_{CE}, which is uncertain (Hurley et al., 2002) and commonly used as a constant $\alpha_{CE} \approx 1$. The final orbital energy and thus the final state of the binary can be calculated using Equation 2.1.

$$E_{bind,i} = \alpha_{CE} \left(E_{orb,f} - E_{orb,i} \right) \tag{2.1}$$

In the absence of RLOF, systems with certain separations survive and shed the envelope. However, with the existence of RLOF, the stars coalesce earlier, which results in the formation of a new star (Hurley et al., 2000). α_{CE} plays a decisive role in the calculation of the binding energy in the envelope, which is decisive in the stellar parameters of the resulting star.

Hurley et al. (2000) discusses that an increase in α_{CE} can produce similar results to the work of Iben and Livio (1993) where a decrease in the envelope binding energy leads to a decrease in the possibility of the stars coalescing. The increase in α_{CE} can be attributed to the existence of other energy sources in addition to the orbital energy (Hurley et al., 2000; Iben and Livio, 1993).

In light of the CE treatment and the significance of α_{CE}, I ran two extra simulations where $\alpha_{CE} = 0.5$ and $\alpha_{CE} = 1.5$ respectively.

WRLOF

In the presence of dense and slow winds, wind mass transfer of increased efficiency can be observed. This event is referred to as WRLOF. `binary_c` allows users to utilize several WRLOF treatments, or completely omit any WRLOF prescription.

In order to observe the effects of increased wind mass transfer efficiency on the binary population, I ran a separate simulation using a q dependent WRLOF prescription. This q dependent treatment is defined in Abate et al. (2013) as a function of q, R_L of the primary and R_d of the wind accretion zone.

$$\beta_{acc} = \min \left\{ \frac{25}{9} q^2 \left[c_1 \left(\frac{R_d}{R_{L,1}} \right)^2 + c_2 \frac{R_d}{R_{L,1}} + c_3 \right], \beta_{acc,max} \right\} \tag{2.2}$$

In this equation, β_{acc} is the accretion efficiency and c_1, c_2 and c_3 are constants.

2.2 System Classification

To classify binary systems of observable parameters that deviate from the single star evolution, I need evolution models of single stars. Using previously generated `MESA` [4] evolution models of single stars, I obtain a baseline for the evolution of stars without binary interactions. MESA (Paxton et al., 2011, 2013, 2015, 2018, 2019) is a 1-D stellar evolution code that calculates stellar evolution tracks, related parameters and detailed internal and global properties.

[4] https://docs.mesastar.org/en/release-r24.03.1/index.html

As discussed in Section 1.3, the binary systems of interest are those with degenerate cores and comparatively overmassive envelopes. These would be stars in binaries that have degenerate cores even though they do not become degenerate while ascending the GB or stars that become degenerate but mass transfer increases the envelope.

With the start of core helium burning at the end of GB, the core degeneracy of the stars become irrelevant (Pols et al., 1998). On the other hand, Deheuvels et al. (2022) shows p and g modes can couple in HG as well, thus the HG phase of stellar evolution can be relevant to analyze the post-MT evolution of stars. Thus, I focus on the core degeneracy between the TAMS and the end of GB phase.

To track the GB ascension of a single star through the core mass, I use the fraction in 2.3. Here, M_{core} is the core mass, $M_{core,TAMS}$ is the core mass at TAMS and $M_{core,TGB}$ is the core mass as the GB evolution comes to an end. Plotting central degeneracy of the star from TAMS until the end of GB provides the evolutionary tracks single stars of various TAMS masses are expected to follow. These tracks are displayed in Figure 2.1.

$$\frac{M_{core} - M_{core,TAMS}}{M_{core,TGB} - M_{core,TAMS}} \tag{2.3}$$

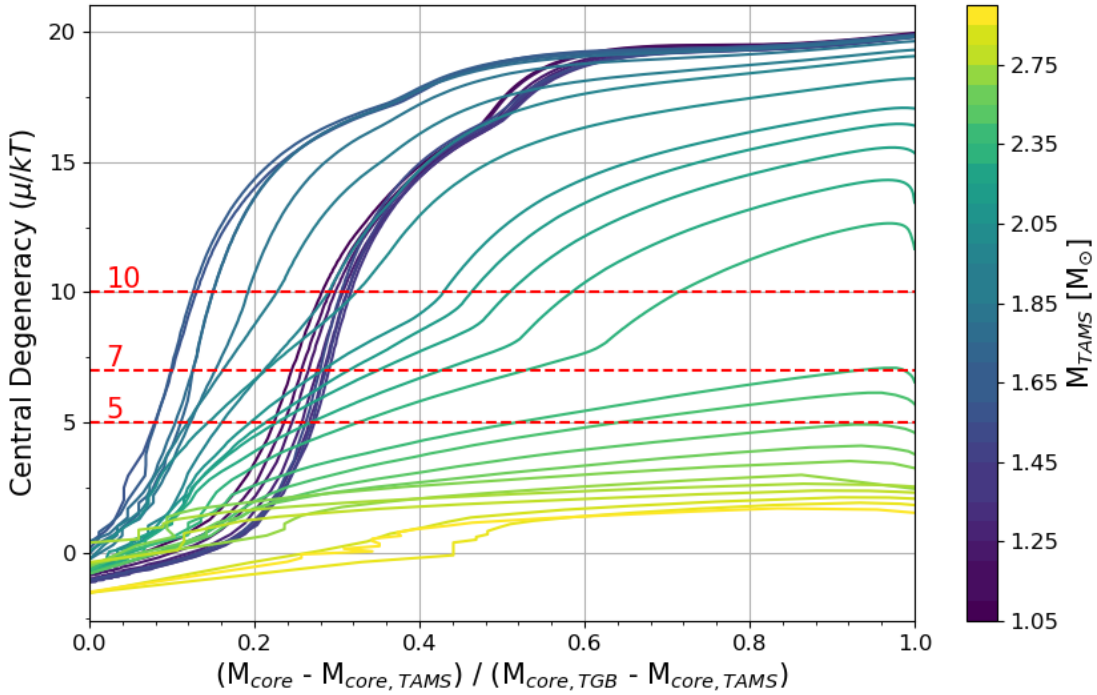

Figure 2.1: Hit criteria generated using `MESA` models.

For my analysis, I refer to the core degeneracy properties of single stars at certain masses described in Pols (2011b) and Aerts (2021). It is known that intermediate-mass stars have non-degenerate cores during hydrogen shell burning and have core massive considerably higher than

that of low-mass stars. Thus, we do not call the cores of stars above certain TAMS mass degenerate. I choose an approximate degeneracy value considering the core properties of single stars and use it as a lower threshold for what we consider a degenerate core. I apply the degeneracy threshold to my binary populations by interpolating the central degeneracy of each star using the MESA data according to their TAMS mass. Following this, I use the core mass values of the stars to trace their post-MS evolution and identify the corresponding degeneracy. Once the degeneracy value exceeds the threshold, I consider the star to have a degenerate core. This process is further discussed in Appendix A.

Another criteria critical to the classification is the MT itself. As discussed in Rui and Fuller (2021), mass transfer allows a star to retain its core degeneracy. Thus, I only set a minimum threshold mass value for the star to have accreted after TAMS. Once a star accretes the threshold mass value while remaining in the GB, I make the assumption that it has retained its degenerate core and now has an overmassive envelope. Note that the amount of MT necessary to cause observable discrepancies is not clear cut. Consequently, I choose an arbitrary mass value of $0.2 M_{\odot}$.

Overall, I use a standard condition with a degeneracy criteria of $7\mu/KT$ and a MT criteria of $0.2 M_{\odot}$. As both of these threshold values are mostly based on approximations and assumptions, the sensitivity of the classification scheme to these values must be analyzed. For this purpose, I use two additional thresholds above and below each one of my criteria. This allows me to have a thorough understanding of the level of uncertainty involved in the classification process. Figure 2.3 shows the five classification conditions I use throughout the study.

Classification Conditions	Degeneracy [μ/KT]	MT [$M_{\odot}$]
Low MT	7	0.1
High MT	7	0.3
Standard	7	0.2
Low Degeneracy	5	0.2
High Degeneracy	10	0.2

Table 2.3: Variations of the binary classification conditions.

Through the degeneracy and MT conditions, I isolate systems of interest and identify whether the primary or the secondary is the star with the overmassive envelope. In this study, I refer to these stars as ”hit” stars. The distinct channels that lead to stars becoming a ”hit” requires an analysis of each distinct binary interaction in the system.

For a thorough look, I identify all interactions that occurred in the system between TAMS and the end of GB. If the system satisfies the previously mentioned MT condition, it is automatically assumed that there is wind MT. If the companion of the hit star fills 99% of its Roche radius, existence of RLOF is assumed. If the companion becomes a Massless Remnant (MR), the stars have merged. The combinations of interactions point to several distinct channels that trigger the core-envelope discrepancy. These channels denoted by 1 or 2 depending on which star is a hit. The channel combinations and the naming conventions used are displayed in Table 2.4.

I also use a hierarchical analysis of wind MT, RLOF and merger events for each system in the population to identify the significance of each type of interaction. I classify any system that

Binary Interactions	Name	
	Primary	Secondary
Merger	MERGER1	MERGER2
Merger & wind MT	MERGER1	MERGER2
Merger & RLOF	MERGER & RLOF1	MERGER & RLOF2
RLOF	RLOF1	RLOF2
RLOF & wind MT	RLOF1	RLOF2
wind MT	WIND1	WIND2

Table 2.4: Variations of the binary classification conditions. The first column displays the possible combinations of binary interactions. The naming conventions are separated into two; the first for cases where the primary is a hit and the second for cases where the secondary is a hit.

experiences a merger event between TAMS and end of GB as a post-merger system, regardless of any wind MT or RLOF presence. I further divide the post-merger systems into MS mergers and evolved mergers. Similarly, I classify systems that experienced RLOF with no mergers as post-RLOF systems. Any system that has not experienced RLOF or merger events are classified as post-wind MT systems. Throughout this study, these three classifications are referred to as MS merger, evolved merger, RLOF and wind respectively.

It is to be noted that once the star reaches the tip of GB, it is no longer considered a hit.

2.3 Reflection to Nature

The initial data obtained from the population represents the frequency of hits and the channels only within the generated population. In order to get a better understanding of how these results would reflect in nature, the data needs to be weighted.

I use Kroupa et al. (1993) to obtain a distribution of stellar birth masses according to the IMF. I apply this distribution within the bounds of the parameter space of my entire population using M_1, q and P, where M_1 and q are uniformly spaced while P is logarithmically spaced. This provides the weights for each system within the population.

Afterwards, I use Kroupa et al. (1993) to model the distribution of unit star forming material (usfm) within a cluster. Using the cluster mass distribution and the weights, I scale the systems within the population with respect to the models of nature. This provides the frequency of hits per usfm in a cluster, as shown in Equation (2.4).

$$\frac{\text{System}}{\text{usfm}[M_\odot]} = \frac{\text{System}}{\text{Systems in Cluster}} \frac{\text{Systems in Cluster}}{\text{usfm}[M_\odot]} \tag{2.4}$$

Weighting each hit system through this process provides insight into the relative significance of binary interactions expected in nature. These weights are used for all analysis relating to the hits throughout this study.

2.4 High-Resolution Analysis

Classifying the systems obtained through the binary_c, I discovered several populations of systems that satisfy the conditions mentioned in Section 2.3. These populations are distinctly concentrated in certain regions of the parameter space.

To get a better look at these populations and the trends in their evolution, I decided to separate the parameter space into smaller grids that cover each one of these populations, but do not overlap with one another. The limits of these boxes in the parameter space are displayed in Table 2.5.

	M_1 $[M_\odot]$	q -	$\log_{10}P$ [days]	Resolution -
Grid 1	1.35–2.6	0.77–1	3.2–4.55	$60 \times 60 \times 60$
Grid 2	0.9–2.4	0.02–0.3	-0.26–1.04	$60 \times 60 \times 60$
Grid 3	0.9–3.7	0.6–0.9	-0.26–0.41	$80 \times 60 \times 30$
Grid 4	0.9–2	0.95–1	0.04–3.2	$60 \times 30 \times 80$
Grid 5	0.9–2	0.75–0.95	1.2–2.1	$60 \times 60 \times 30$
Grid 6	2.1–2.3	0.5–0.6	0.5–0.9	$20 \times 20 \times 10$

Table 2.5: Parameter boundaries for high resolution grids.

While this grid approach provides a large increase in resolution, whether it can provide drastically new perspectives for the entire population is questionable. This analysis and its advantages are further discussed in Section 3.5.

Chapter 3

Results and Discussion

3.1 Fiducial Physics Case

Under the standard classification scheme, analysis of the binary interactions experienced by the hit star and where in the initial parameter space these cases correspond to imply the existence of several distinct channels. Figure 3.4 illustrates the initial M_1, q and P values of the hits throughout the parameter space.

There are various populations concentrated in the different parts of the parameter space with distinct trends of binary interactions. Binaries with large periods and close mass ratios experience RLOF and wind MT. The companion in these systems are all TPAGB stars. Conducting single star analysis on these systems to get a better understanding of the channel itself (Appendix B), it can be seen that the primary completes its CHeB phase while the secondary is in HG. Upon reaching TPAGB, the primary sheds its envelope to become a Carbon Oxygen White Dwarf (COWD). In this process, the secondary is able to accrete a small amount of material, enough to have core-envelope discrepancy.

Binaries of low q and P show a tendency to merge into the primary, making it a hit. The corresponding companions are all low mass MS stars. This is a distinct example of the low mass MS - GB merger that pushes the GB star to retain its degenerate core at higher masses. On the other hand, cases of a primary merging with a high-mass MS secondary are seen to occur in very close binaries of relatively high q.

Another distinct channel is the events where the secondary becomes a hit and merges with a CHeB primary. These occur in binaries within a very small range of P. However, these events span across a large part of the parameter space for both the primary mass and q.

Finally, the rest of the initial parameter space is dominated by primaries merging with HG stars or GB stars. They are seen to occur across most of the P range and the lower half of the M_1 range. On the other hand, these mergers are seen to strictly occur at very high q binaries. These are consistent with the BSE treatment of mergers where two merging HG or two merging GB stars result in the formation of a GB star.

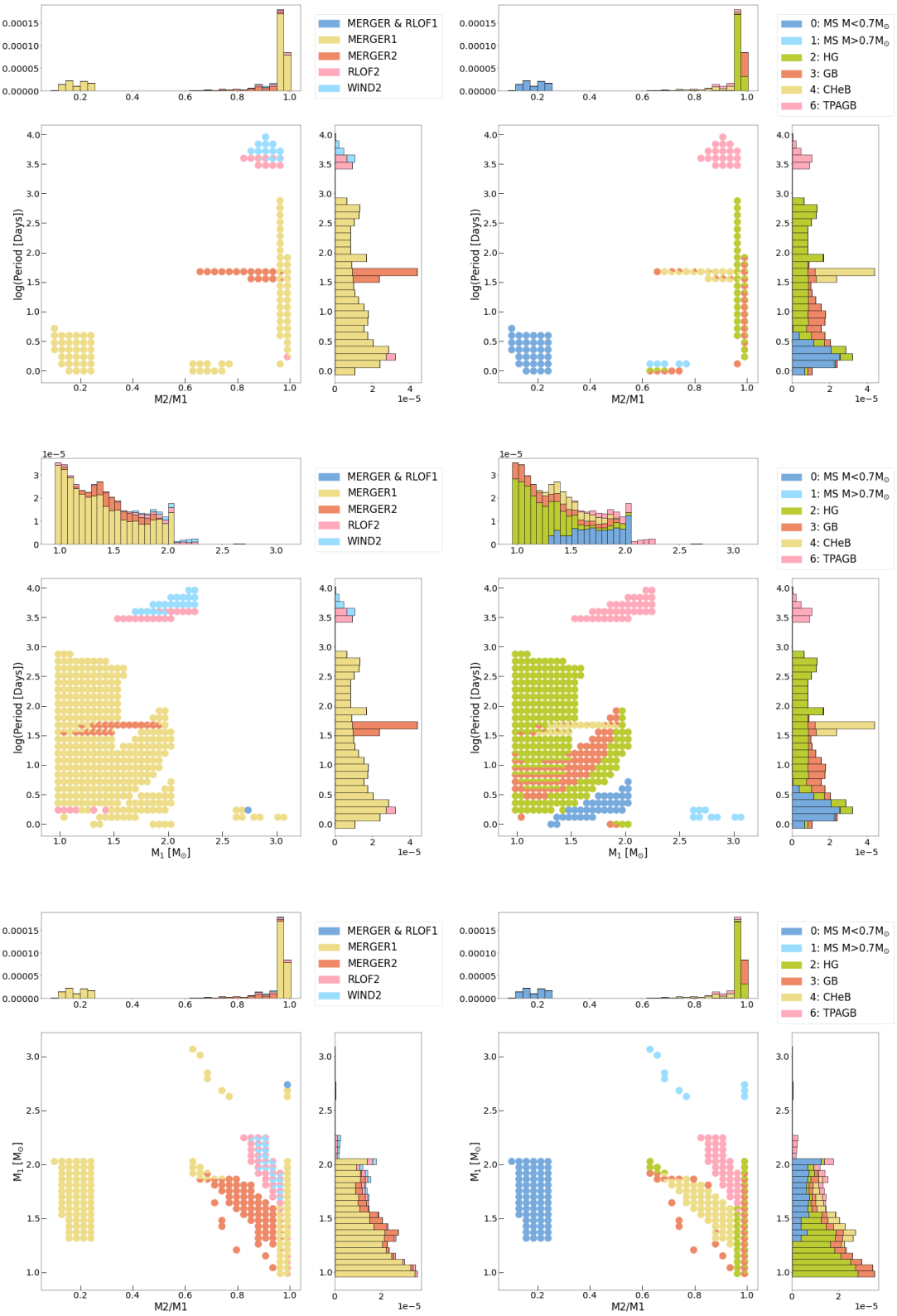

Figure 3.1: The left column is the binary interaction classification for each system. The right column is the color coded according to the stellar type of the companion star right before the hit star satisfied the standard classification condition. The data is weighted per usfm with the histograms showing the relative significance of each event across the parameter space.

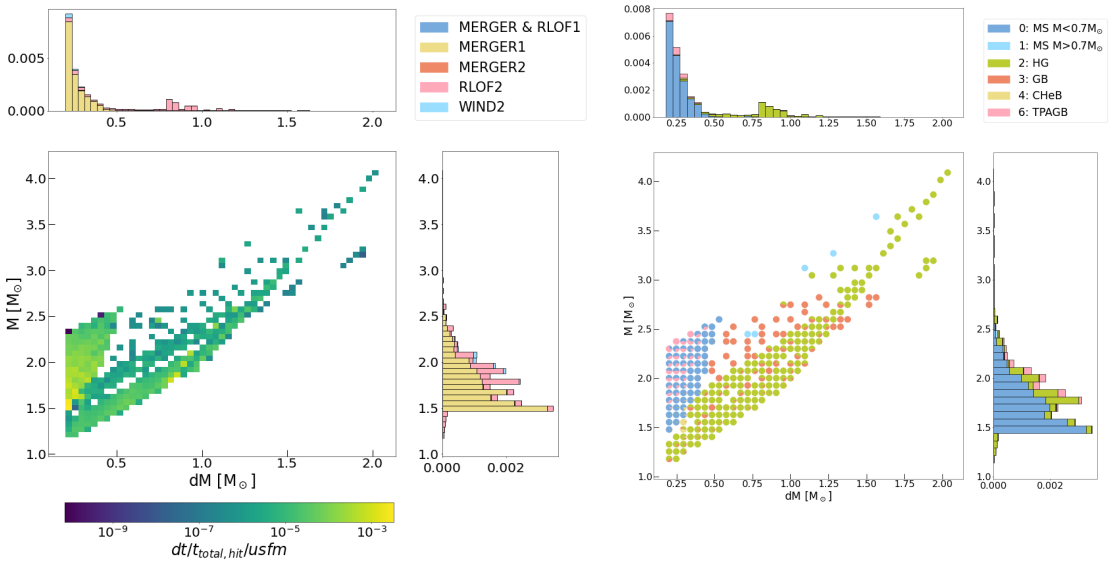

Figure 3.2: The evolution of the mass of the hit and the mass transferred since TAMS, calculated from the moment the star becomes a hit until reaches the end of GB. 2-D histogram on the left shows where across the parameter range the data is accumulated the most. The data is classified according to the binary interactions, which are color coded and displayed on the 1-D histograms. The scatter plot on the right is color coded by the companion stellar type before the star becomes a hit. The data is weighted by the fractional change in time while the star is a hit per usfm.

To probe the trends during the period of evolution while the star is a hit, 2-D histograms and scatter plots illustrating the companion star's stellar type right before the star becomes a hit are used. Two examples of these plots are displayed in Figure 3.2 for the mass of the hit and the mass transferred since TAMS.

Primaries merging with a low-mass MS companion are seen to transfer less mass compared to the HG mergers of the secondary. However, their relative significance is drastically higher as seen in the 1-D histograms. Unlike the MERGER1 cases, MERGER2 events are seen to experience larger MT and evolve to higher masses until the tip of GB. RLOF events from a TPAGB donor star are seen to only accrete very low masses. Combined with the single star analysis, this is a clear implication of non-conservative MT.

Comparing the weighted sums displayed in the histograms for the scatter plots in Figure 3.4 and Figure 3.2, it can be seen that the inclusion of time in the weighting process changes the observed significance of these events. To have a clear look on these relative significance, the weighted time and systems are calculated for both the hierarchical classification method and the broad classification method.

	System Number	Total Time [t_{tot}/usfm]	Weighted Systems [sys/usfm]
WIND	47	5.462e−4	1.089e−5
RLOF	67	5.662e−3	2.051e−5
MERGER	781	1.783e−2	3.933e−4

Table 3.1: Hierarchical for baseline physics case.

From Table 3.1, the population is seen to be dominated by mergers both in terms of the systems born and the total time spent as a hit. The weighted systems for RLOF are twice that of wind MT and the time spent as a hit is 10 times larger for RLOF. This makes RLOF the second most significant event across the population.

	System Number -	Weighted Systems [sys/usfm]	Total Time [t_{tot}/usfm]	Wind Time [t_{wind}/usfm]	RLOF Time [t_{RLOF}/usfm]	Merger Time [t_{merger}/usfm]
RLOF2	67	2.051e−5	5.662e−3	3.575e−3	2.087e−3	0
WIND2	47	1.089e−5	5.462e−4	5.510e−4	0	0
MERGER & RLOF1	1	1.123e−7	2.399e−6	0	0	2.396e−6
MERGER1	670	3.442e−4	1.772e−2	0	0	1.772e−2
MERGER2	110	4.891e−5	9.947e−5	0	0	9.913e−5

Table 3.2: Non-hierarchical for fiducial physics case.

Table 3.2 shows that most of the mergers dominating the population are mergers of the primary. These spend drastically more time as hits compared to all the other binary interactions. They correspond to the mergers where the companion is a low-mass MS, as previously displayed.

3.1.1 Degeneracy Threshold

To probe the sensitivity of the population to the degeneracy threshold chosen, I analyze the same population from the fiducial case, only changing the degeneracy threshold.

At a low degeneracy of 0.5, the number of hits show an increase compared to the fiducial case. However, the increase in the weighted time and weighted systems are not very drastic. From Table 3.4, we can see that cases of RLOF, wind MT and mergers of the primary have increased. However, mergers of the secondary are completely unaffected by this change.

	System Number	Total Time [t_{tot}/usfm]	Weighted Systems [sys/usfm]
WIND	76	6.340e−4	1.543e−5
RLOF	87	5.725e−3	2.364e−5
MERGER	881	1.810e−2	4.128e−4

Table 3.3: Hierarchical for low degen case.

	System Number	Weighted Systems [sys/usfm]	Total Time [t_{tot}/usfm]	Wind Time [t_{wind}/usfm]	RLOF Time [t_{RLOF}/usfm]	Merger Time [t_{merger}/usfm]
RLOF2	87	2.364e−5	5.725e−3	3.637e−3	2.087e−3	0
WIND2	76	1.543e−5	6.340e−4	6.408e−4	0	0
MERGER & RLOF1	1	1.123e−7	2.399e−6	0	0	2.396e−6
MERGER1	770	3.637e−4	1.800e−2	0	0	1.799e−2
MERGER2	110	4.891e−5	9.947e−5	0	0	9.913e−5

Table 3.4: Non-hierarchical for low degen case.

For an increased degeneracy threshold of 10, no change is observed in the weighted time and weighted system calculations compared to the fiducial case. No new systems become hits and the hit times remain unchanged. This points to a decreased sensitivity to higher degeneracy thresholds and is further discussed in Section **??**.

3.1.2 Mass Transfer Threshold

Unlike the degeneracy condition, toggling the mass transfer condition creates drastic effects in the identification of hits. At a decreased MT threshold of $0.1M_{\odot}$, it becomes easier for stars to satisfy the condition to become a hit. Consequently, we see a drastic increase in the amount of hits. Figure 3.5 shows that there is a drastic increase in the weighted time compared to the increase in the weighted systems. This is especially prominent for the wind MT events. This increases the significance of wind MT effects on the star by almost a fraction of 5.

	System Number	Total Time [t_{tot}/usfm]	Weighted Systems [sys/usfm]
WIND	166	2.711e−3	4.112e−5
RLOF	101	8.136e−3	3.215e−5
MERGER	950	2.360e−2	4.488e−4

Table 3.5: Hierarchical for low mt case.

On the other hand, increasing the MT condition to $0.3M_{\odot}$ gets rid of many of the systems previously logged as hits in the fiducial case. The binary interaction most affected by this criteria is once again the wind MT. Table 3.6 shows that the number of wind MT cases drop down

to more than one tenth of those in the fiducial case.

	System Number	Total Time [t_{tot}/usfm]	Weighted Systems [sys/usfm]
WIND	3	1.384E-05	5.336E-07
RLOF	31	4.781E-03	1.081E-05
MERGER	592	4.269E-03	3.180E-04

Table 3.6: Hierarchical for high mt case.

3.2 CE Physics

In the fiducial case, the α_{CE} is set to 1 as per Tout et al. (1997). To understand the effects of a lower α_{CM}, I analyze the simulation I ran with $\alpha_{CE} = 0.5$. The change in α_{CE} has no effect on the RLOF and wind MT events. A slight increase in the overall mergers is observed according to Table 3.7.

	System Number	Total Time [t_{tot}/usfm]	Weighted Systems [sys/usfm]
WIND	47	5.462E-04	1.089E-05
RLOF	67	5.607E-03	2.045E-05
MERGER	827	1.891E-02	4.360E-04

Table 3.7: Hierarchical for alpha 0.5 case.

The most dramatic effect observed is the changes within the merger events. Compared to the fiducial case, Table 3.8 shows that almost all mergers of the secondary have now switched to mergers of the primary.

	System Number	Weighted Systems [sys/usfm]	Total Time [t_{tot}/usfm]	Wind Time [t_{wind}/usfm]	RLOF Time [t_{RLOF}/usfm]	Merger Time [t_{merger}/usfm]
RLOF2	67	2.045E-05	5.607E-03	3.546E-03	2.061E-03	0
WIND2	47	1.089E-05	5.462E-04	5.510E-04	0	0
MERGER & RLOF1	1	1.123E-07	2.399E-06	0	0	2.396E-06
MERGER & RLOF2	2	1.668E-06	2.642E-04	2.587E-04	1.347E-04	5.572E-06
MERGER1	822	4.325E-04	1.864E-02	0	0	1.863E-02
MERGER2	2	1.730E-06	3.947E-06	0	0	3.933E-06

Table 3.8: Non-hierarchical for alpha 0.5 case.

With this change in α_{CE}, the secondary mergers seem to have turned into primary mergers while retaining the type of channel where two GB or two HG stars merge to form a GB star.

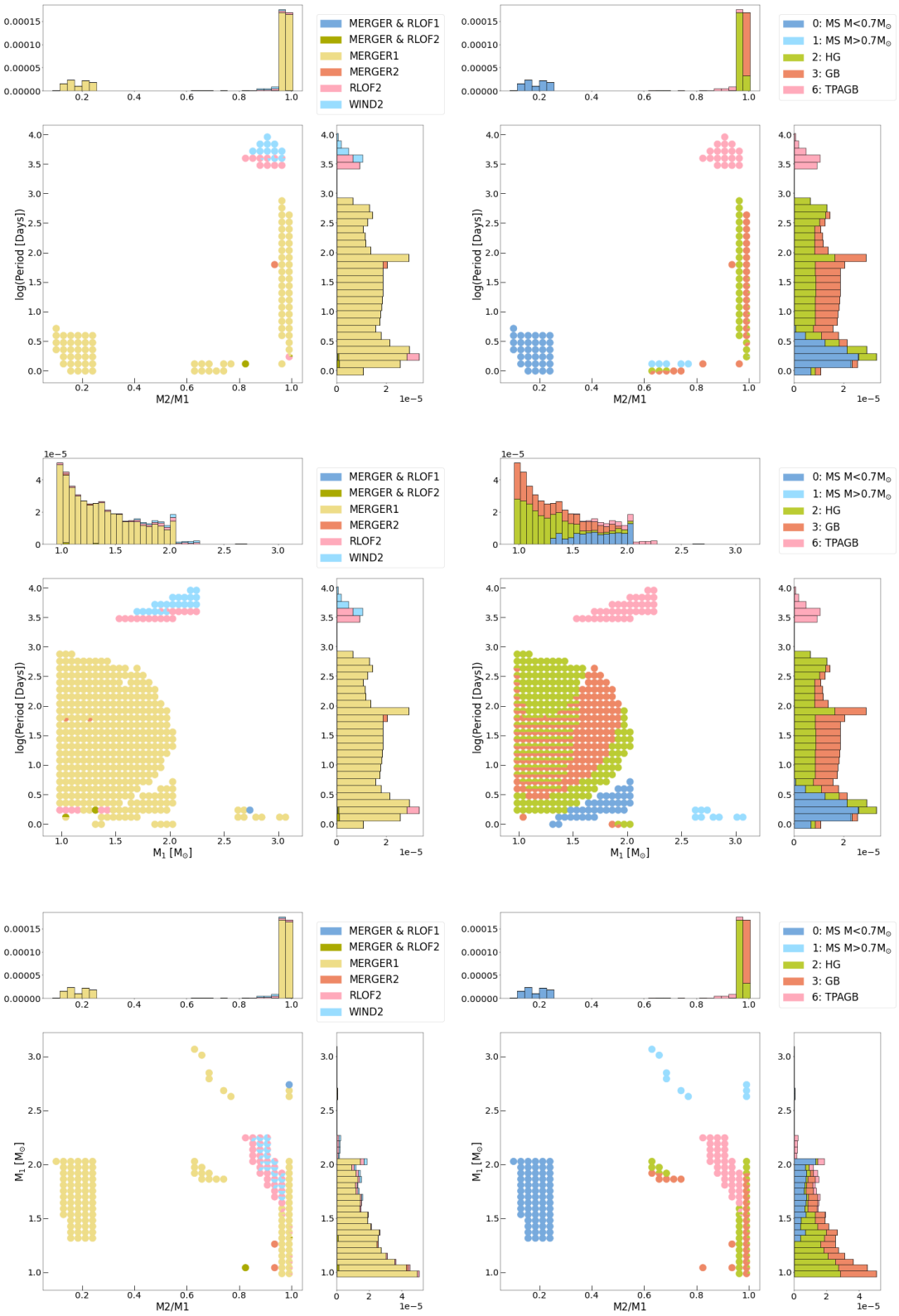

Figure 3.3: Population distribution plots for $\alpha_{CE} = 0.5$. The left column is the binary interaction classification for each system. The right column is the color coded according to the stellar type of the companion star right before the hit star satisfied the standard classification condition. The data is weighted per usfm with the histograms showing the relative significance of each event across the parameter space.

To probe the other end and check whether the population corresponds to the behavior described by Iben and Livio (1993); Hurley et al. (2002), I generate and analyze a population with $\alpha_{CE} = 1.5$. This change, too, increases the amount of mergers in the population. However, unlike the lower α_{CE} case, the weighted time is lower than that of the fiducial physics case.

	System Number	Total Time [t_{tot}/usfm]	Weighted Systems [sys/usfm]
WIND	47	5.462E-04	1.089E-05
RLOF	68	5.864E-03	2.107E-05
MERGER	937	1.330E-02	4.401E-04

Table 3.9: Hierarchical for alpha 1.5 case.

A major difference between this population and the population with lower α_{CE} is the distribution of the merger types. Table 3.10 shows a relatively balanced ratio between the primary mergers and the secondary mergers unlike the previous simulation where almost all secondary mergers became primary mergers. However, in terms of the weighted time, primary mergers are the most significant binary interaction in this population as well.

	System Number	Weighted Systems [sys/usfm]	Total Time [t_{tot}/usfm]	Wind Time [t_{wind}/usfm]	RLOF Time [t_{RLOF}/usfm]	Merger Time [t_{merger}/usfm]
RLOF2	68	2.107E-05	5.864E-03	3.668E-03	2.196E-03	0
WIND2	47	1.089E-05	5.462E-04	5.510E-04	0	0
MERGER & RLOF1	1	1.123E-07	2.399E-06	0	0	2.396E-06
MERGER1	596	3.061E-04	1.302E-02	0	0	1.301E-02
MERGER2	340	1.339E-04	2.790E-04	0	0	2.787E-04

Table 3.10: Non-hierarchical for $\alpha_{CE} = 1.5$ case.

3.3 WRLOF Physics

Enabling the WRLOF settings lead to a drastic increase in the detected wind MT events. In terms of weighted time, wind MT events dominate this population. The WRLOF prescription also results in an increase of RLOF and mergers.

	System Number	Total Time [t_{tot}/usfm]	Weighted Systems [sys/usfm]
WIND	1006	3.453E-02	3.114E-04
RLOF	127	6.202E-03	3.240E-05
MERGER	794	1.784E-02	4.039E-04

Table 3.11: Hierarchical for WRLOF case.

Especially for high q binaries with large periods, there is a significant increase in the wind MT and RLOF cases. This leads to the wind and RLOF events dominating the parameter space in terms of observability.

3.4 Metallicity

Changing metallicity from solar metallicity to one tenth of solar metallicity affects all aspects of stellar evolution. In terms of binary interactions, the most significant change is the increase in mergers. Both primary and secondary mergers show considerable increase compared to the fiducial case.

Due to the complexity of the effects of metallicity on single star evolution alone, its application to a binary system is just as complex.

3.5 High Resolution Analysis

Upon generating 6 grids of high resolution binary systems, I used the standard classification scheme to analyze the population. In this analysis, it was seen that there are many edge cases for each grid that sometimes expand out of the grid. However, detailed analysis is required to identify is the increase in resolution is actually providing a detailed look into unseen yet significant systems, or if this is a result of oversampling.

	System Number	Total Time [t_{tot}/usfm]	Weighted Systems [sys/usfm]
WIND	47	2.829E-04	1.097E-05
RLOF	70	7.689E-04	1.861E-05
MERGER	1217	2.199E-02	5.084E-04

Table 3.12: Hierarchical for metallicity case.

One of the shortcomings of this analysis method is the fact that each grid is sampled differently, making it hard to merge every single one of the grids together to get a thorough look. A detailed probing with well designed grids and a way to move past the computational weight of this very data-loaded analysis will be beneficial for future work.

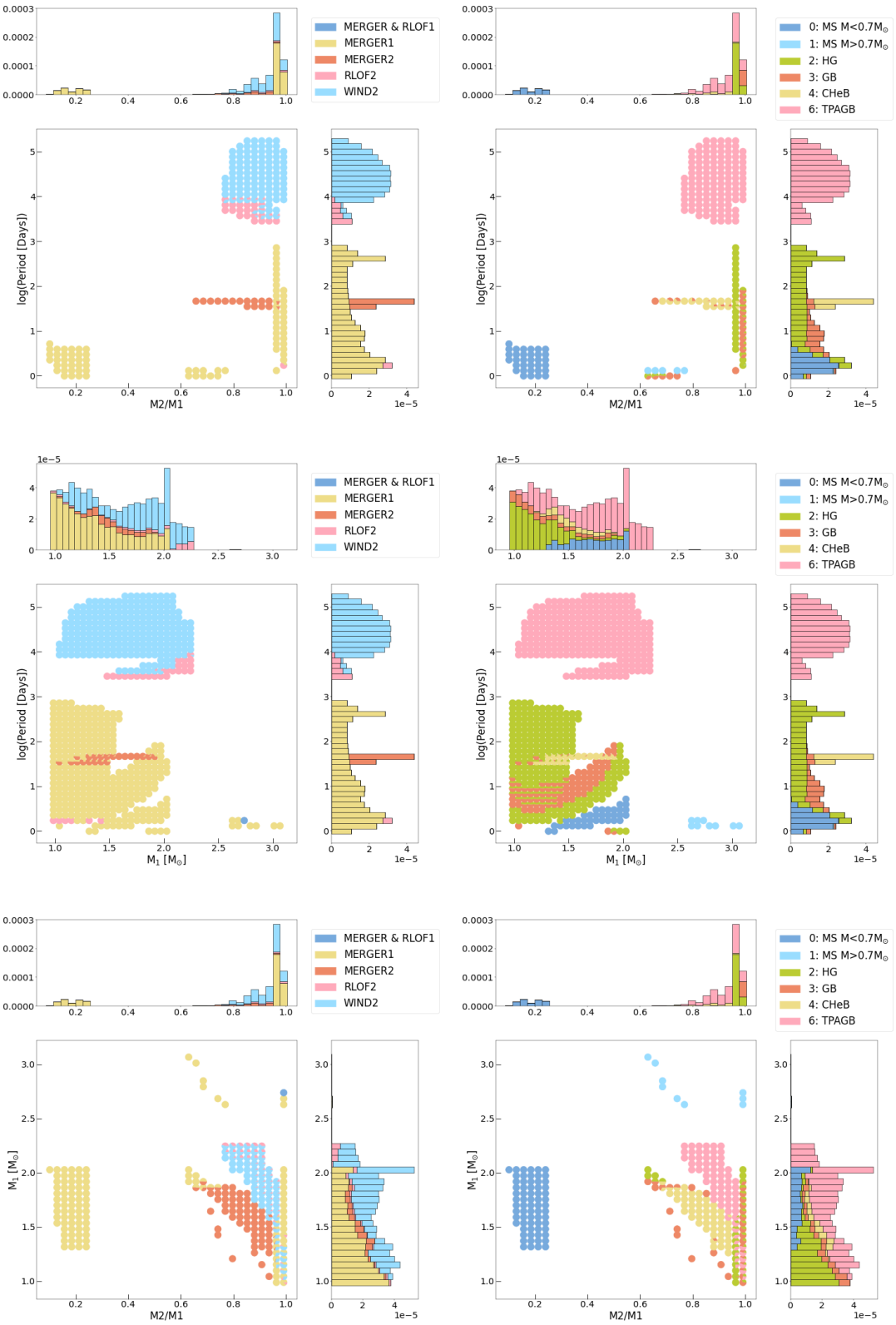

Figure 3.4: Population distribution plots for the population where WRLOF is present. The left column is the binary interaction classification for each system. The right column is the color coded according to the stellar type of the companion star right before the hit star satisfied the standard classification condition. The data is weighted per usfm with the histograms showing the relative significance of each event across the parameter space.

Chapter 4

Conclusions

In this study, the possible observability of post-MT binary systems with core-envelope discrepancies were studied in detail through binary population synthesis. Populations of binaries were generated using `binary_c`. Alternative populations were used to probe the effects of α_{CE}, WRLOF and metallicity on the binary interactions. A classification scheme was designed using thresholds on the minimum mass transferred in the system and the central degeneracy of the stars. Through these classifications, possible channels leading to the formation of a star that has a degenerate core and an overmassive envelope were identified. These systems were then weighed according to the stellar and binary birth probabilities, providing numerical support for the possibility of the observation of these systems and the significance of these channels.

I was able to identify several distinct channels across the population which lead to the formation of a post-MT star. The runaway material from TPAGBs accreted onto the companion proved to be a common channel for high q binaries with large separations. This channel accounted for almost all of the RLOF and wind MT events. In close low q binaries, mergers were dominant for stars with a low-mass MS companion, corroborating the findings of (Rui and Fuller, 2021). The secondary mergers were frequently cases of mergers with CHeB companions. The broadest channel was primary mergers for high q binaries where both stars are HG or GB.

I tested the robustness of the classification scheme by varying the MT and degeneracy thresholds. The decrease in the degeneracy condition did introduce additional systems but the increase of the degeneracy condition did not change the classifications of any of the systems. This was attributed to the initial threshold of 7 marking a boundary between the degeneracy curves of TAMS masses beyond which the stars did not experience a considerable increase in central degeneracy along the GB. Thus, the classification scheme was minimally affected by variations in the degeneracy. On the other hand, the MT threshold proved to be a critical parameter for the classifications. An increase in the MT threshold drastically decreased the hits while a decrease increased them. The binary interaction most sensitive to the MT criterion was seen to be wind MT. The various physics cases provided results mostly corresponding to the expectations based on Abate et al. (2013), Hurley et al. (2000) and Iben and Livio (1993).

4.1 Future Work

Due to the sensitivity of the classification method to the MT threshold, the effects of this threshold can be further probed. In a similar vein, due to the metallicity affecting many aspects of stellar evolution, a detailed analysis of its effects on binary interactions could not be conducted within the scope of this study. The effect of metallicity can be studied considering the evolution of individual binaries and utilizing many multiplicity values.

Focusing on certain grids on the parameter space where certain channels are densely populated and generating populations in these grids with high resolution proved to existence of many edge cases that were not resolved in the fiducial population. However, utilization of these grids requires detailed calculations for the resolution in each grid for the grids to be compatible with one another. It is quite computationally taxing due to the large amounts of hits. Furthermore, there remains a possibility of the edge cases observed being redundant when the population is weighted to reflect observability. Understanding whether this approach can provide a new and distinct perspective requires rigorous work in the future.

Bibliography

Abate, C., Pols, O. R., Izzard, R. G., Mohamed, S. S., and de Mink, S. E. (2013). Wind Roche-lobe overflow: Application to carbon-enhanced metal-poor stars. *A&A*, 552:A26.

Abt, H. A. (1983). Normal and abnormal binary frequencies. *ARA&A*, 21:343–372.

Aerts, C. (2021). Stellar structure and evolution.

Aerts, C., Christensen-Dalsgaard, J., and Kurtz, D. W. (2010). *Asteroseismology*.

Agrawal, P., Hurley, J., Stevenson, S., Rodriguez, C. L., Szécsi, D., and Kemp, A. (2023). Modelling stellar evolution in mass-transferring binaries and gravitational-wave progenitors with METISSE. *MNRAS*, 525(1):933–951.

Chandra (2015). Pulsating variable stars and the hertzsprung-russell (h-r) diagram.

Claeys, J. S. W., Pols, O. R., Izzard, R. G., Vink, J., and Verbunt, F. W. M. (2014). Theoretical uncertainties of the Type Ia supernova rate. *A&A*, 563:A83.

Comerford, T. A. F. and Izzard, R. G. (2020). Estimating the outcomes of common envelope evolution in triple stellar systems. *MNRAS*, 498(2):2957–2967.

Comins, N. F. and Kaufmann, W. J. (2008). *Discovering the Universe Eighth Edition*.

De Rosa, R. J., Bulger, J., Patience, J., Leland, B., Macintosh, B., Schneider, A., Song, I., Marois, C., Graham, J. R., Bessell, M., and Doyon, R. (2011). The Volume-limited A-Star (VAST) survey - I. Companions and the unexpected X-ray detection of B6-A7 stars. *MNRAS*, 415(1):854–866.

Deheuvels, S., Ballot, J., Gehan, C., and Mosser, B. (2022). Seismic signature of electron degeneracy in the core of red giants: Hints for mass transfer between close red-giant companions. *A&A*, 659:A106.

Deheuvels, S. and Michel, E. (2011). Constraints on the structure of the core of subgiants via mixed modes: the case of HD 49385. *A&A*, 535:A91.

Dewi, J. D. M. and Tauris, T. M. (2000). On the energy equation and efficiency parameter of the common envelope evolution. *A&A*, 360:1043–1051.

Duchêne, G. and Kraus, A. (2013). Stellar Multiplicity. *ARA&A*, 51(1):269–310.

Eldridge, J. J., Stanway, E. R., Xiao, L., McClelland, L. A. S., Taylor, G., Ng, M., Greis, S. M. L., and Bray, J. C. (2017). Binary Population and Spectral Synthesis Version 2.1: Construction, Observational Verification, and New Results. *PASA*, 34:e058.

Fragos, T., Andrews, J. J., Bavera, S. S., Berry, C. P. L., Coughlin, S., Dotter, A., Giri, P., Kalogera, V., Katsaggelos, A., Kovlakas, K., Lalvani, S., Misra, D., Srivastava, P. M., Qin, Y., Rocha, K. A., Román-Garza, J., Serra, J. G., Stahle, P., Sun, M., Teng, X., Trajcevski, G., Tran, N. H., Xing, Z., Zapartas, E., and Zevin, M. (2023). POSYDON: A General-purpose Population Synthesis Code with Detailed Binary-evolution Simulations. *ApJS*, 264(2):45.

García, R. A. and Ballot, J. (2019). Asteroseismology of solar-type stars. *Living Reviews in Solar Physics*, 16(1):4.

Hekker, S., Aerts, C., De Ridder, J., and Carrier, F. (2006). Pulsations detected in the line profile variations of red giants. Modelling of line moments, line bisector and line shape. *A&A*, 458(3):931–940.

Hurley, J. R., Pols, O. R., and Tout, C. A. (2000). Comprehensive analytic formulae for stellar evolution as a function of mass and metallicity. *MNRAS*, 315(3):543–569.

Hurley, J. R., Tout, C. A., and Pols, O. R. (2002). Evolution of binary stars and the effect of tides on binary populations. *MNRAS*, 329(4):897–928.

Iben, Icko, J. and Livio, M. (1993). Common Envelopes in Binary Star Evolution. *PASP*, 105:1373.

Izzard, R. G., Dray, L. M., Karakas, A. I., Lugaro, M., and Tout, C. A. (2006). Population nucleosynthesis in single and binary stars. I. Model. *A&A*, 460(2):565–572.

Izzard, R. G., Glebbeek, E., Stancliffe, R. J., and Pols, O. R. (2009). Population synthesis of binary carbon-enhanced metal-poor stars. *A&A*, 508(3):1359–1374.

Izzard, R. G., Preece, H., Jofre, P., Halabi, G. M., Masseron, T., and Tout, C. A. (2018). Binary stars in the Galactic thick disc. *MNRAS*, 473(3):2984–2999.

Izzard, R. G., Tout, C. A., Karakas, A. I., and Pols, O. R. (2004). A new synthetic model for asymptotic giant branch stars. *MNRAS*, 350(2):407–426.

Karakas, A. I., Lattanzio, J. C., and Pols, O. R. (2002). Parameterising the Third Dredge-up in Asymptotic Giant Branch Stars. *PASA*, 19(4):515–526.

Kopal, Z. (1978). *Dynamics of close binary systems*.

Kopal, Z. (1989). *The Roche Problem and its significance for double-star astronomy*, volume 152.

Kouwenhoven, M. B. N., Brown, A. G. A., Zinnecker, H., Kaper, L., and Portegies Zwart, S. F. (2005). The primordial binary population. I. A near-infrared adaptive optics search for close visual companions to A star members of Scorpius OB2. *A&A*, 430:137–154.

Kroupa, P., Tout, C. A., and Gilmore, G. (1993). The Distribution of Low-Mass Stars in the Galactic Disc. *MNRAS*, 262:545–587.

Li, Y., Bedding, T. R., Murphy, S. J., Stello, D., Chen, Y., Huber, D., Joyce, M., Marks, D., Zhang, X., Bi, S., Colman, I. L., Hayden, M. R., Hey, D. R., Li, G., Montet, B. T., Sharma, S., and Wu, Y. (2022). Discovery of post-mass-transfer helium-burning red giants using asteroseismology. *Nature Astronomy*, 6:673–680.

Misra, D., Fragos, T., Tauris, T. M., Zapartas, E., and Aguilera-Dena, D. R. (2020). The origin of pulsating ultra-luminous X-ray sources: Low- and intermediate-mass X-ray binaries containing neutron star accretors. *A&A*, 642:A174.

Paxton, B., Bildsten, L., Dotter, A., Herwig, F., Lesaffre, P., and Timmes, F. (2011). Modules for Experiments in Stellar Astrophysics (MESA). *ApJS*, 192:3.

Paxton, B., Cantiello, M., Arras, P., Bildsten, L., Brown, E. F., Dotter, A., Mankovich, C., Montgomery, M. H., Stello, D., Timmes, F. X., and Townsend, R. (2013). Modules for Experiments in Stellar Astrophysics (MESA): Planets, Oscillations, Rotation, and Massive Stars. *ApJS*, 208:4.

Paxton, B., Marchant, P., Schwab, J., Bauer, E. B., Bildsten, L., Cantiello, M., Dessart, L., Farmer, R., Hu, H., Langer, N., Townsend, R. H. D., Townsley, D. M., and Timmes, F. X. (2015). Modules for Experiments in Stellar Astrophysics (MESA): Binaries, Pulsations, and Explosions. *ApJS*, 220:15.

Paxton, B., Schwab, J., Bauer, E. B., Bildsten, L., Blinnikov, S., Duffell, P., Farmer, R., Goldberg, J. A., Marchant, P., Sorokina, E., Thoul, A., Townsend, R. H. D., and Timmes, F. X. (2018). Modules for Experiments in Stellar Astrophysics (MESA): Convective Boundaries, Element Diffusion, and Massive Star Explosions. *ApJS*, 234:34.

Paxton, B., Smolec, R., Schwab, J., Gautschy, A., Bildsten, L., Cantiello, M., Dotter, A., Farmer, R., Goldberg, J. A., Jermyn, A. S., Kanbur, S. M., Marchant, P., Thoul, A., Townsend, R. H. D., Wolf, W. M., Zhang, M., and Timmes, F. X. (2019). Modules for Experiments in Stellar Astrophysics (MESA): Pulsating Variable Stars, Rotation, Convective Boundaries, and Energy Conservation. *ApJS*, 243(1):10.

Podsiadlowski, P., Joss, P. C., and Hsu, J. J. L. (1992). Presupernova Evolution in Massive Interacting Binaries. *ApJ*, 391:246.

Pols, O. (2011a). Binary stars.

Pols, O. (2011b). Stellar structure and evolution.

Pols, O. R., Schröder, K.-P., Hurley, J. R., Tout, C. A., and Eggleton, P. P. (1998). Stellar evolution models for Z = 0.0001 to 0.03. *MNRAS*, 298(2):525–536.

Reimers, D. (1975). Circumstellar absorption lines and mass loss from red giants. *Memoires of the Societe Royale des Sciences de Liege*, 8:369–382.

Rui, N. Z. and Fuller, J. (2021). Asteroseismic fingerprints of stellar mergers. *MNRAS*, 508(2):1618–1631.

Salpeter, E. E. (1955). The Luminosity Function and Stellar Evolution. *ApJ*, 121:161.

Sana, H. (2017). The multiplicity of massive stars: a 2016 view. In Eldridge, J. J., Bray, J. C., McClelland, L. A. S., and Xiao, L., editors, *The Lives and Death-Throes of Massive Stars*, volume 329, pages 110–117.

Sana, H., de Mink, S. E., de Koter, A., Langer, N., Evans, C. J., Gieles, M., Gosset, E., Izzard, R. G., Le Bouquin, J. B., and Schneider, F. R. N. (2012). Binary Interaction Dominates the Evolution of Massive Stars. *Science*, 337(6093):444.

Tassoul, M. (1980). Asymptotic approximations for stellar nonradial pulsations. *ApJS*, 43:469–490.

Tassoul, M., Fontaine, G., and Winget, D. E. (1990). Evolutionary Models for Pulsation Studies of White Dwarfs. *ApJS*, 72:335.

Tauris, T. M. and Dewi, J. D. M. (2001). Research Note On the binding energy parameter of common envelope evolution. Dependency on the definition of the stellar core boundary during spiral-in. *A&A*, 369:170–173.

Tout, C. A., Aarseth, S. J., Pols, O. R., and Eggleton, P. P. (1997). Rapid binary star evolution for N-body simulations and population synthesis. *MNRAS*, 291(4):732–748.

Vassiliadis, E. and Wood, P. R. (1993). Evolution of Low- and Intermediate-Mass Stars to the End of the Asymptotic Giant Branch with Mass Loss. *ApJ*, 413:641.

Appendices

Appendix A

MESA Models

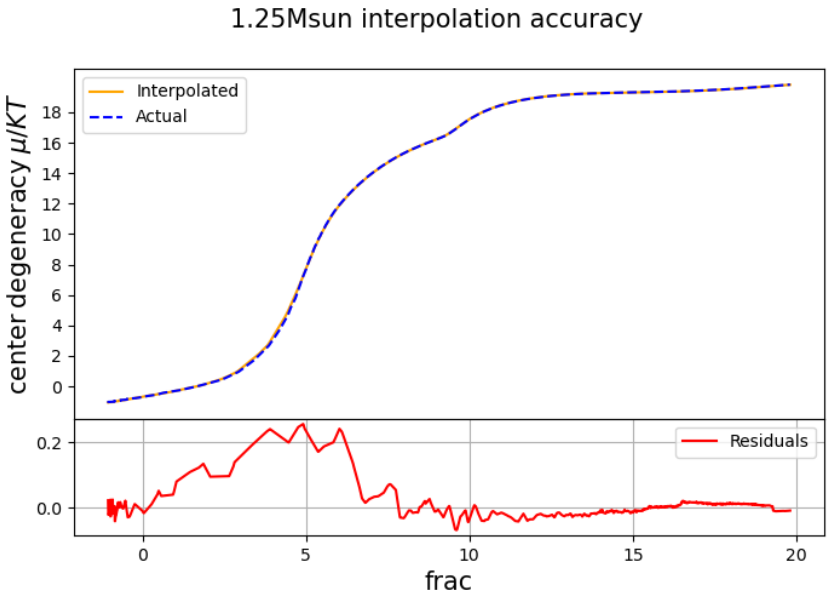

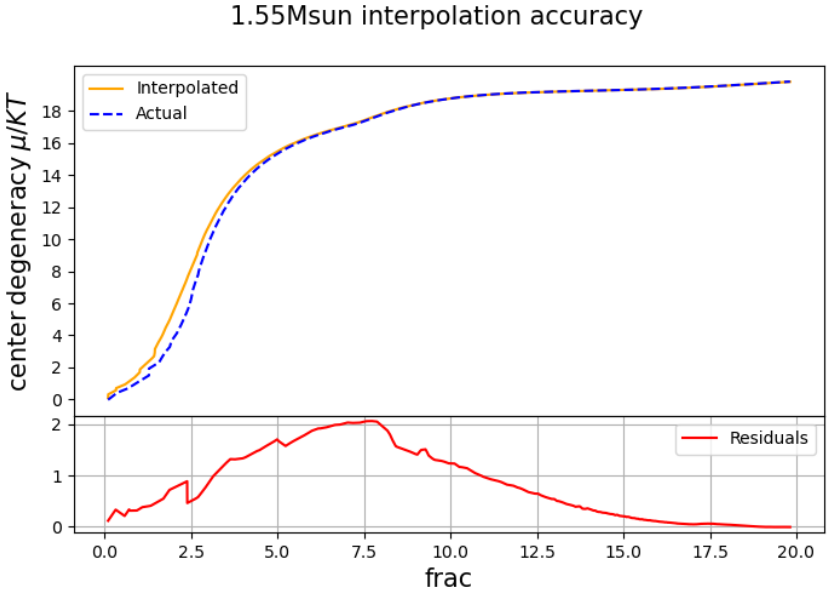

Appendix B

Single Star Analysis

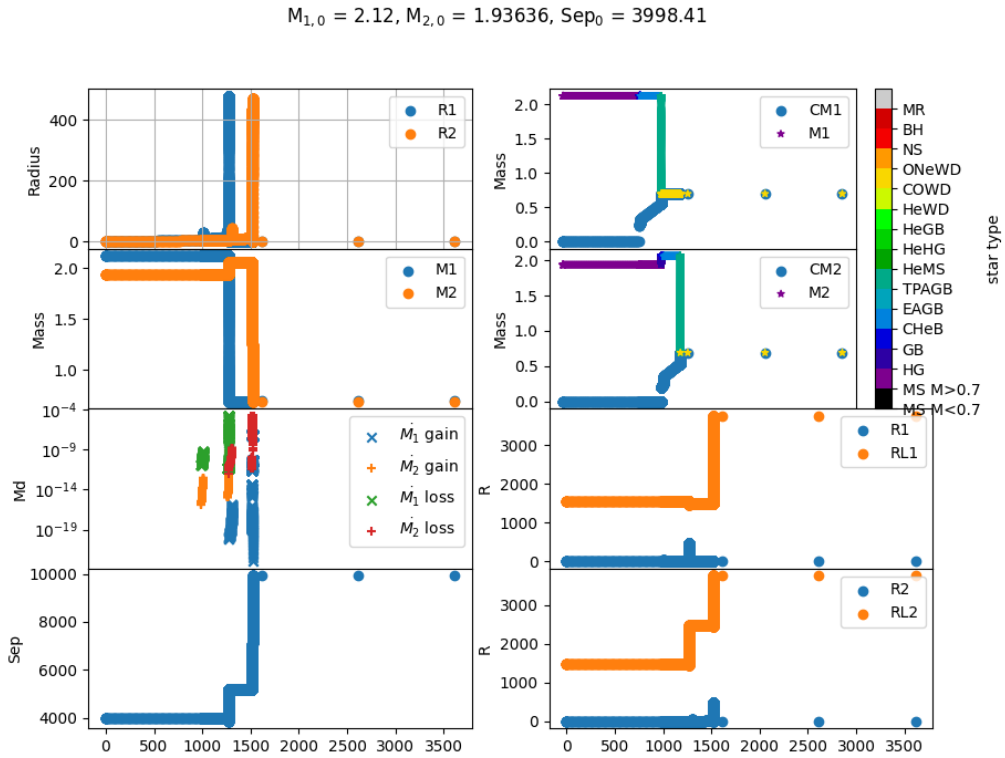

AFDELING
Straat nr bus 0000
3000 LEUVEN, BELGIË
tel. + 32 16 00 00 00
fax + 32 16 00 00 00
www.kuleuven.be